NANO LETTERS

Letter

pubs.acs.org/NanoLett

Effect of the Core/Shell Interface on Auger Recombination Evaluated by Single-Quantum-Dot Spectroscopy

Young-Shin Park, Wan Ki Bae,[‡] Lazaro A. Padilha,[†] Jeffrey M. Pietryga, and Victor I. Klimov*

Chemistry Division, Los Alamos National Laboratory, Los Alamos, New Mexico 87545, United States

Supporting Information

ABSTRACT: Previous single-particle spectroscopic studies of colloidal quantum dots have indicated a significant spread in biexciton lifetimes across an ensemble of nominally identical nanocrystals. It has been speculated that in addition to dot-to-dot variation in physical dimensions, this spread is contributed to by variations in the structure of the quantum dot interface, which controls the shape of the confinement potential. Here, we directly evaluate the effect of the composition of the core–shell interface on single- and multiexciton dynamics via side-by-side measurements of individual core–shell CdSe/CdS nanocrystals with a sharp versus smooth (graded) interface. To realize the latter type of structures we incorporate a $CdSe_xS_{1-x}$ alloy layer of controlled composition and thickness between the CdSe core and the CdS shell. We observe that while having essentially no effect on single-exciton decay, the interfacial alloy layer leads to a systematic increase in biexciton lifetimes, which correlates with the increase in the biexciton emission efficiency, as inferred from two-photon correlation measurements. These observations provide direct experimental evidence that in addition to the size of the quantum dot, its interfacial properties also significantly affect the rate of Auger recombination, which governs biexciton decay. These findings help rationalize previous observations of a significant heterogeneity in the biexciton lifetimes across similarly sized quantum dots and should facilitate the development of "Auger-recombination-free" colloidal nanostructures for a range of applications from lasers and light-emitting diodes to photodetectors and solar cells.

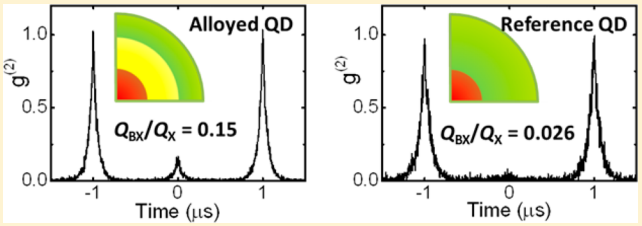

KEYWORDS: *Semiconductor nanocrystal, quantum dot, core/shell, alloyed interface, biexciton, Auger recombination, second-order intensity correlation function*

Multicarrier dynamics in nanocrystal quantum dots (QDs) are usually governed by nonradiative Auger recombination wherein the energy of an electron–hole pair is not converted into a photon but is instead transferred to a third carrier.[1] This process is believed to be responsible for the low emissivity of charged excitations (e.g., trions) and multiexcitons in QDs and is often invoked to explain photoluminescence (PL) intermittency (blinking) detected in single-QD studies.[2,3] Auger recombination complicates applications of QDs in light-emitting diodes (LEDs),[4] single-photon and photon-pair sources,[5,6] photovoltaic (PV) devices,[7] and especially lasers,[8] as all of these applications either directly rely on emission from multiexcitons (lasers and photon-pair sources) or are influenced by the effects of charging (LEDs, PVs, and single-photon emitters). Therefore, the development of "Auger-recombination-free" QDs is an important current challenge in the field of colloidal nanostructures.

In monocomponent QDs, the Auger recombination time is controlled by particle dimensions and scales linearly with particle volume (known as a universal "*V*-scaling").[9] While exhibiting a quick increase with QD size, Auger lifetimes are still short (subnanosecond time scale) relative to single-exciton radiative lifetimes, even in large QDs with sizes approaching that of a bulk exciton. An alternative approach to reducing Auger decay rates is based on inducing spatial separation of electrons and holes, which reduces wave function overlap for the ground-state electron and hole participating in the recombination event. This strategy was explored, for example, using type-II core/shell QDs[10,11] and dot-in-rod nanostructures.[12] Reduced electron–hole overlap is also one of the reasons for Auger decay suppression in so-called "giant" quasi-type-II CdSe/CdS core/shell QDs (g-QDs) wherein electrons are delocalized over the entire structure while holes are tightly confined within the small core.[13−15]

Calculations by Cragg and Efros,[16] and more recently by Climente et al.,[17] have suggested that in addition to QD size the shape of the confinement potential also has a significant effect on the Auger decay rate. Specifically, it was shown that by "smoothing" the confinement potential one can reduce the overlap between the initial and the final state of the carrier excited during Auger recombination, which can lead to orders-of-magnitude reduction in the rate of this process. The effect of potential smoothing on Auger decay was invoked to explain suppression of blinking in alloyed QDs[18] and was likely responsible for increased multiexciton emission intensity in CdTe/CdSe QDs.[19] It was also cited as one of the reasons for a

Received: May 21, 2013
Revised: December 10, 2013
Published: January 7, 2014

   dx.doi.org/10.1021/nl403289w | *Nano Lett.* 2014, 14, 396−402

wide distribution in biexciton emission quantum yields (QYs) across an ensemble of similarly sized quantum dots.[15] More recently, the correlation between unintentional interfacial alloying detected by fluorescence line narrowing and suppression of Auger recombination was reported for CdSe/CdS NCs with a varied shell thickness.[20]

Our most recent studies provided even more direct evidence for a significant effect of the shape of the confinement potential on the rate of Auger recombination.[21] The focus of this published work was on a novel synthesis of CdSe/CdS QDs that allowed for a much faster growth of a thick CdS shell compared to a more traditional successive ionic layer adsorption and reaction (SILAR) method.[13,22,23] Application of the new technique allowed us to avoid unintentional alloying at the CdSe/CdS interface and synthesize structures with two distinct interfaces: one with a sharp core−shell boundary and the other with a well-defined $CdSe_xS_{1-x}$ alloy layer incorporated between the core and the shell. A preliminary spectroscopic study of these two types of samples indicated that while the alloy layer did not have a significant effect on single exciton decay it did affect biexciton dynamics, which were considerably slower in samples with alloyed interfaces.

In the present Letter, we use these newly developed samples to directly evaluate the effect of controlled interfacial alloying on the rate of nonradiative Auger recombination in individual QDs by analyzing biexciton photoluminescence (PL) efficiencies (Q_{BX}) via second-order intensity correlation ($g^{(2)}$) measurements. Using this method we examine overall structure-dependent trends in the QD ensemble and also analyze dot-to-dot variations in Q_{BX} as well as exciton (τ_X) and biexciton (τ_{BX}) lifetimes. Our studies indicate that the biexciton PL QY in alloyed QDs can be up to ~10 times higher than that in the core/shell samples with a sharp CdSe/CdS interface. These results are validated by independent single-dot measurements of biexciton dynamics that also show a considerable increase in τ_{BX} upon interfacial alloying. Furthermore, we observe a remarkable quantitative agreement between the Q_{BX} values derived by the $g^{(2)}$-method and those inferred from the measured τ_{BX} and τ_X time constants. Finally, a systematic investigation of ~100 individual QDs of both types (with either sharp or alloyed interfaces) shows that the CdS shell thickness has only a minor effect on biexciton emission QY. This is in contrast to a dramatic effect of the incorporation of even a thin interfacial alloy layer, which leads to a manifold increase in Q_{BX}. We also observe that a controlled modification of a core/shell interface allows for a more uniform suppression of Auger decay across the QD ensemble as compared to more traditional g-QDs with more poorly defined CdSe/CdS interfaces. All of these findings point toward a significant role of the shape of the confinement potential in Auger recombination and indicate the possibility of controlling this effect via appropriate engineering of QD interfaces.

Biexciton Auger recombination can occur via two processes whereby the electron−hole recombination energy is transferred to either an electron (referred here to as a negative trion pathway) or a hole (positive trion pathway) with characteristic time constants τ_{A,X^-} and τ_{A,X^+}, respectively. Accordingly, the biexciton Auger lifetime, τ_{BX}, can be expressed as $1/\tau_{A,BX} = 2/\tau_{A,X^+} + 2/\tau_{A,X^-}$. For core-only QDs, Auger lifetimes follow volume scaling, which in the case of spherical particles of radius R can be presented as $\tau_{A,X^-}, \tau_{A,X^+}, \tau_{A,BX} \propto R^3$. To generalize this expression for the case of heterostructured QDs we assume that each of the radii in the R^3 term represents the effective radius of localization of one of the carriers participating in Auger decay. In this case, the R^3 scaling can be rewritten as $1/\tau_{A,BX} \propto [1/(R_h^2R_e) + 1/(R_hR_e^2)]$, where R_e and R_h are the effective radii of electron and hole localization, respectively. The first and the second term in this expression describe, respectively, the positive and the negative trion pathway in biexciton recombination with characteristic time constants $\tau_{X^+} \propto R_h^2R_e$ and $\tau_{X^-} \propto R_hR_e^2$.

In thick-shell CdSe/CdS g-QDs, the electron is delocalized over the entire nanostructure while the hole is strongly confined to the core, which results in a regime where R_e is significantly greater than R_h (Figure 1a). Therefore, the rate of

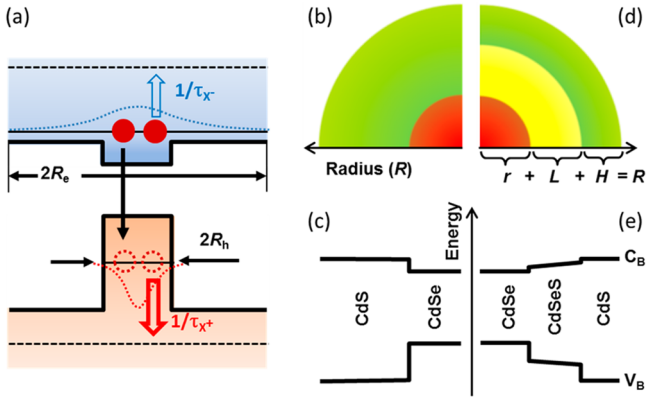

Figure 1. (a) Positive (X^+) and negative (X^-) trion pathways in biexciton Auger recombination. Schematic illustration of internal structures and confinement potentials of reference core/shell CdSe/CdS (b,c) and alloyed CdSe/$CdSe_xS_{1-x}$/CdS QDs (d,e). In this study, the core radius (r = 1.5 nm) and the thickness of the alloyed layer (L = 1.5 nm) are fixed while the thickness of the CdS shell is varied.

the X^- Auger pathway is much lower than that of the X^+ pathway, and as a result the PL QY of a negative trion in g-NCs can be comparable to the QY of a neutral exciton.[24] This leads to an interesting phenomenon of "lifetime-blinking" when the fluctuation of a g-QD between the neutral and the negatively charged exciton states is not accompanied by intensity fluctuations but instead leads to a fluctuating PL lifetime.[24] These considerations also imply that in g-QDs the biexciton Auger decay is dominated by the fast positive trion pathway in which recombination of the electron−hole pair is accompanied by excitation of a band-edge hole to a higher-energy state. Because in g-QDs holes are primarily confined to the core, the rate of the X^+ Auger pathway can be controlled by shape of the core/shell potential, which according to calculations[16,17] has a significant effect on the overlap between the initial and the final state of the hole excited in the Auger process. Specifically, by smoothing this potential (via, e.g., interfacial alloying) one can achieve a significant reduction in the rate of the X^+ pathway and hence the rate of biexciton Auger recombination.

To study the effect of the core/shell interface on Auger recombination, we have fabricated two types of QDs using a novel fast shell growth method[21] (see Supporting Information, Section 1). As was discussed above, it allows us to realize structures with either a sharp core/shell interface (no intentional or unintentional interfacial alloying) or an alloyed interface when a layer of $CdSe_xS_{1-x}$ of a controlled thickness and composition is introduced between the core and the shell. Below, we will refer to these structures as to "reference" (Figures 1b,c) and "alloyed" (Figures 1d,e) QDs, respectively.

dx.doi.org/10.1021/nl403289w | Nano Lett. 2014, 14, 396−402

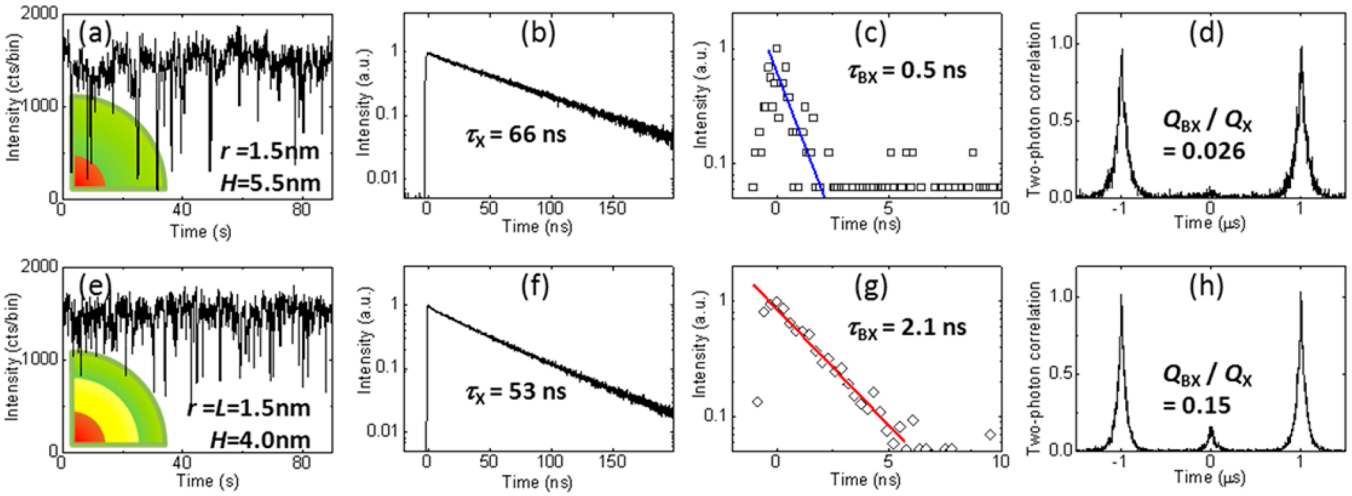

Figure 2. PL intensity trajectories, TCSPC and two-photon correlation measurements of individual reference (a–d) and alloyed (e–h) core/shell QDs with the same core radii (1.5 nm) and the same total radii (7 nm); the thickness of the $CdSe_xS_{1-x}$ layer in the alloyed dot is 1.5 nm. (a,e) PL intensity trajectories with a time bin of 40 ms. (b,f) Single-exciton dynamics. (c,g) Biexciton dynamics extracted from the two-channel TCSPC data. (d,h) Two-photon correlation measurements. All data were obtained simultaneously from a single measurement for each QD using a pump fluence of 0.64 fJ/pulse, which corresponds to $\langle N \rangle = 0.1$.

For all samples, the CdSe core radius (r) is 1.5 nm and the CdS shell thickness (H) varies from 1.5 to 5.5 nm, which spans the range from standard thin-shell QDs to g-QDs with an ultrathick outer layer. In the alloyed QDs, the core and shell regions are separated by an L = 1.5 nm thick alloy layer with x of ~0.5 (x decreases slightly toward the periphery of the alloy layer; see Supporting Information Figure S3). Assuming that the height of the potential barrier is linearly proportional to the CdS fraction, the alloyed layer can be schematically described by an intermediate step in the overall confinement potential as shown in Figure 1e.

For confocal micro-PL experiments, the QD sample was first diluted in hexane and then drop-cast onto quartz substrates with a QD density as low as $0.1/\mu m^2$. A pulsed laser (PicoQuant; 488 nm wavelength and 40 ps pulse duration) was used to excite individual QDs. The laser repetition rate (1 MHz) was chosen to be low enough to allow for complete relaxation of PL before the arrival of the next laser pulse. An oil immersion objective lens (60×, 1.3 numerical aperture) was used for both focusing laser pulses and collecting PL from individual QDs. For time-correlated single-photon counting (TCSPC) and $g^{(2)}$ measurements, we used a standard Hanbury Brown and Twiss setup where QD PL photons were divided by a 50/50 beam splitter into two independent optical paths and detected with two single-photon avalanche photodiodes (APDs) (~350 ps time resolution). Utilizing the multichannel, time-tagged, time-resolved (TTTR) mode provided by our TCSPC module (PicoQuant), we recorded both the macrotime (time elapsed from the start of a measurement) and the microtime (time relative to a laser pulse) for each detector independently. Through postprocessing of the TTTR data, we could extract the PL-intensity time trajectory, the PL dynamics of both excitons and biexcitons, and the second-order intensity correlation function simultaneously from a single measurement.[25,26] Specifically, in order to obtain the biexciton dynamics for an individual QD we consider only the events when two photons were detected (one on each detector) for the same excitation pulse; these are the same events that contribute to the coincidence counts in the zero-delay $g^{(2)}$ peak. By assigning the first of the arrived photons to biexciton recombination and the second to recombination of a single exciton (remaining after biexciton decay), we extract the biexciton dynamics for individual QDs. All measurements were performed at room temperature for spectrally integrated emission without separating PL signals from single excitons and biexcitons.

Figure 2 shows representative results of measurements of PL intensity trajectories, lifetimes, and second-order intensity correlation for a reference core/shell QD (a–d) with H = 5.5 nm (corresponds to ~16 monolayers, MLs, of CdS) and an alloyed QD (e–h) with L = 1.5 nm and H = 4.0 nm; both QDs have the same core radii (r = 1.5 nm) and the same total radii (R = 7.0 nm) (see Figure S4 of Supporting Information for single-QD PL spectra of these samples). The measurements were conducted using low pump intensity such that the average QD excitonic occupancy per excitation pulse, $\langle N \rangle$, is approximately 0.1 (see Supporting Information, Section 6).

Both QDs feature nearly nonblinking PL (on-time fraction greater than 95%), as was previously observed for thick-shell ("giant") QDs with ≥16 CdS MLs[13] (see also Figure S7 of Supporting Information for the analysis of lifetime trajectories of the same QDs). Single exciton dynamics (Figures 2b,f) for both QDs are also similar and are characterized by time constants, τ_X, of 66 ns (reference QD) and 53 ns (alloyed QD). These lifetimes are longer than those in core-only CdSe QDs (~20 ns)[27] due to delocalization of the electron wave function into the thick CdS shell, which reduces its overlap with the core-localized hole.[28] In contrast to the similarities seen in single-exciton decay, the biexciton lifetime for the alloyed QD (τ_{BX} = 2.1 ns; a red line in Figure 2g) is considerably longer than that for the reference core/shell QD (τ_{BX} = 0.5 ns; a blue line in Figure 2c) (see Supporting Information Figure S5 for more examples illustrating a considerable lengthening of biexciton decay in alloyed QDs). The slowdown of biexciton dynamics can be attributed to suppression of nonradiative Auger recombination in the alloyed structure with a smoothened confinement potential. Such behavior, lengthening of a biexciton lifetime for an unchanged single-exciton lifetime, is consistent with expectations for Auger decay suppression resulting from reduced overlap between the initial and the final

dx.doi.org/10.1021/nl403289w | Nano Lett. 2014, 14, 396–402

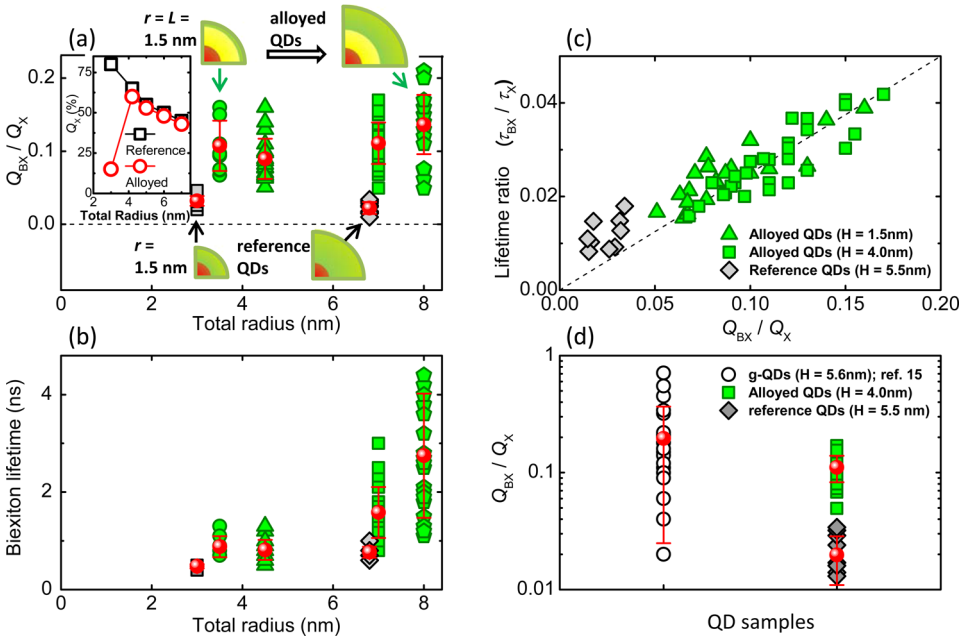

Figure 3. (a) CdS shell-thickness dependence of normalized biexciton PL QYs and (b) corresponding lifetimes for the reference core/shell (gray) and the alloyed (green) QDs. For alloyed QDs, the CdS-shell thicknesses are 0.5 (circles), 1.5 (triangles), 4.0 (squares), and 5.0 nm (pentagons). For the reference QDs, H = 1.0 nm (squares) and 5.5 nm (diamonds). For R = 7.0 nm, gray diamonds are slightly shifted left for clarity. Solid red circles show average values and bars correspond to standard deviations. An inset in (a) shows ensemble single-exciton PL QYs for both types of QDs as a function of total radius. (c) The plot of the lifetime ratios (τ_{BX}/τ_X) versus QY ratios (Q_{BX}/Q_X) for ~50 individual QDs from the reference core/shell (gray diamonds) and alloyed (green symbols) samples. Experimental data closely follow a linear dependence with a slope of 1/4 (dashed line). (d) Comparison of Q_{BX}/Q_X dot-to-dot variability among similarly sized QD samples: alloyed QDs (green squares), reference QDs (gray diamonds), and g-QDs (open circles, from ref 15).

state of a carrier excited in the course of Auger recombination. Indeed, while affecting the biexciton (or trion) Auger decay rate this overlap integral does not affect single-exciton dynamics.

Suppressed nonradiative Auger rate in alloyed NCs should lead to an enhancement in the biexciton PL QY. As demonstrated previously,[15,29,30] Q_{BX} of individual QDs can be measured from the second-order intensity correlation functions, $g^{(2)}$, by comparing the area ratio between the central (time delay zero) and the side (time delay equal to laser pulse-to-pulse separation) peaks. This $g^{(2)}$ ratio measured in the weak excitation limit ($\langle N\rangle \ll 1$) provides a direct measure of the ratio of the PL QYs of biexcitons and single excitons (Q_{BX}/Q_X). Pump-power dependent measurements of $g^{(2)}$ (Figure S6a of Supporting Information) indicate that for the pump fluences used in our studies ($\langle N\rangle$ of ca. 0.1), the center-to-side peak $g^{(2)}$ area ratio is $\langle N\rangle$-independent and hence indeed is defined by Q_{BX}/Q_X. We would like to point out that the contribution from higher-order multiexcitons to the center peak of the $g^{(2)}$ function is less than 2%, which is well below the noise level in our measurements (see Supporting Information, Section 7).

As shown in Figure 2h, the $g^{(2)}$ function of the alloyed QD shows incomplete antibunching with an area ratio of 0.15 which implies Q_{BX}/Q_X = 0.15. This result is very similar to one obtained previously for g-QDs, where Q_{BX}/Q_X of 0.18 on average was inferred from the measurements of >20 individual CdSe/CdS QDs with a 16 ML thick shell.[15] Taking into account that the radiative decay rate of a biexciton is four times that of an exciton[15,31] we obtain $\tau_{BX} = (\tau_X/4)(Q_{BX}/Q_X)$ = 2.0 ns, which is in excellent agreement with the value derived from the direct measurement of biexciton dynamics (Figure 2g).

In contrast to a fairly large zero-delay $g^{(2)}$ peak observed for the alloyed QD, the $g^{(2)}$ measurement of the reference QD shows strong antibunching (central- to side-peak area ratio of 0.03), indicating a negligibly small biexciton PL QY due to highly efficient nonradiative Auger decay. The biexciton lifetime inferred from this measurement, τ_{BX} = 0.5 ns, is also in good agreement with the value obtained from direct measurements of biexciton dynamics (Figure 2c). More examples of consistent correlations between the results of the $g^{(2)}$ and PL dynamics measurements are given below.

Next, we perform an analysis of measurements on ~100 individual QDs from both reference and alloyed samples aimed to identify shell-thickness dependent trends in the PL QYs (Figure 3a) and the biexciton lifetimes (Figure 3b). Figure 3a displays the biexciton-to-exciton ratio of PL QYs derived from single-dot $g^{(2)}$ measurements as a function of total radius, R, for both alloyed (green symbols) and reference (gray symbols) QDs; both type of samples have the same core radii (r = 1.5 nm) and all alloyed QDs have the same thickness of the intermediate $CdSe_xS_{1-x}$ layer (L = 1.5 nm). In the inset, we also compare single-exciton PL yields (plotted vs R) for these two types of samples derived from ensemble measurements.[21] For the smallest dots (R = 3 nm), the alloyed sample exhibits a lower single-exciton PL QY than the reference sample (~15 vs ~80%) as it does not have CdS capping (H = 0) and therefore is more strongly affected by surface-related trapping/recombination. The addition of even a fairly thin, 1 nm CdS outer layer (R = 4 nm) considerably improves the PL QY of the alloyed QDs (up to >60%) that becomes almost the same as that of the reference samples. A close similarity between the QYs is maintained for larger R (that is, larger shell thicknesses) as both samples exhibit a gradual decline in the Q_X value until it reaches ~45% for R = 7 nm. As Q_X is controlled by single-exciton recombination, these results reinforce the statement made

dx.doi.org/10.1021/nl403289w | Nano Lett. 2014, 14, 396−402

earlier in the paper that introduction of an intermediate alloy layer does not significantly affect single-exciton dynamics, that is, it does not modify either exciton radiative decay or nonradaitive recombination (except for the smallest-R sample without CdS coating).

In contrast to these similarities in size-dependent trends for single excitons, the trends observed for biexcitons are dramatically different between the two types of samples. Specifically, for the reference core/shell dots, independent of their shell thickness, the biexciton PL QY is always low ($Q_{BX}/Q_X < 0.03$), and further it does not exhibit any appreciable variation with H, as illustrated in Figure 3a for samples with H = 1.5 and 5.5 nm. This is a direct consequence of highly efficient Auger recombination dominated by the X^+ pathway. The rate of this pathway is primarily dependent on the radius of hole localization, which is essentially defined by the core size, and does not significantly vary with shell thickness.

The H-dependence of Q_{BX}/Q_X observed for alloyed samples is significantly different. In this case, even for the thinnest CdS shell (L = 1.5 nm, H = 0.5 nm; solid green circles in Figure 3a), we already observe a fairly high Q_{BX} (up to ∼0.16 for some of the dots and 0.11 on average), suggesting that intrinsic Auger decay is greatly suppressed due to a "smoothened" interfacial potential. Interestingly, a further increase in the shell thickness does not appreciably affect the average value of Q_{BX}/Q_X. Even for the thickest-shell samples (H = 5 nm) it is only ∼40% larger than in the sample with H = 0.5 nm. This observation implies that the presence of the alloyed layer, rather than the CdS thickness, plays the defining role in Auger decay suppression. Further, these results also suggest that the spread in the Q_{BX} values among the QDs with a nominally identical total size (∼26% for alloyed QDs with R = 7 nm; Figure 3a) arises primarily from dot-to-dot variations in the structure of the interfacial alloy layer (that is, its thickness and composition) rather than variations in shell thickness. This argument is also supported by QD size analysis by transmission electron microscopy (TEM) (see Figure S2 of Supporting Information). This analysis indicates that the size dispersion of alloyed QDs increases with increasing shell thickness. Specifically, while the standard deviation of the QD radii for sample with R = 3 nm is 6.6% it increases to 12% for dots with R = 7 nm. Importantly, this increase in the spread of the QD size does not seem to result in any appreciable increase in the Q_{BX}/Q_X variability, which would be expected for the standard volume-scaling of Auger lifetimes. Instead, the variation of the Q_{BX}/Q_X ratio remains about ∼30% regardless of the CdS shell thickness. This fact reemphasizes that in this type of QDs, it is the structure of the alloyed layer rather than the CdS shell thickness that controls biexciton Auger decay.

The key role of interfacial alloy in suppression of Auger decay derived from the analysis of the $g^{(2)}$-based Q_{BX}/Q_X measurements is further supported by single-QD TCSPC studies of biexciton lifetimes (Figure 3b). The measurements of reference core/shell QDs indicate that independent of shell thickness, τ_{BX} is always short (subnanoseconds time scale) and shows only a slight increase with shell thickness. For example, as shown in Figure 3b, τ_{BX} = 0.48 ns for H = 1.5 nm and it increases to 0.77 ns for H = 5.5 nm. This lifetime lengthening is similar to that observed in single-exciton decay[15,28] and is likely explained by the same reason, which is the reduction in the electron−hole overlap due to delocalization of the electron over the increasing volume of the QD.

The alloyed QDs exhibit distinct size-dependent trends. Even in a thin-shell alloyed sample with H = 0.5 nm (total radius R = 3.5 nm) some of the dots show τ_{BX} up to ∼1.3 ns, which is nearly twice as large as the longest biexciton time constant measured for a thick-shell reference sample having H = 5.5 nm (R = 7 nm). The biexciton lifetime in alloyed QDs grows further with increasing shell thickness and can be as long as 4.4 ns in samples with H = 5.0 nm. These results point again toward significant suppression of biexciton Auger recombination associated with the presence of the intermediate alloy layer.

In addition to leading to similar qualitative conclusions, the results of the $g^{(2)}$ and TCSPC measurements are also in excellent quantitative agreement, as specifically seen in terms of the above-mentioned relation between lifetimes and QYs, $\tau_{BX}/\tau_X = (1/4)(Q_{BX}/Q_X)$. In Figure 3c, we present the results of our $g^{(2)}$ and TCSPC measurements for both reference and alloyed QDs in the form of a τ_{BX}/τ_X versus Q_{BX}/Q_X plot. We observe a remarkable correlation between the two quantities, which manifests in a close alignment of the experimental data points along the expected linear dependence with slope 1/4. A slight vertical offset of the data for reference samples that are characterized by short τ_{BX} arises from an apparent artificial lengthening of biexciton lifetimes due to the fairly long response time of our APDs (∼350 ps). As one might anticipate based on previous discussions, the data for the reference (gray diamonds) and alloyed (green symbols) QDs occupy two distinct regions of the plot that correspond, respectively, to lower and higher values of τ_{BX}/τ_X and Q_{BX}/Q_X. This once again illustrates a significant difference between the properties of biexcitons in these two types of the QDs.

Finally, we would like to discuss the relationship between the results of the present work and those of our previous studies of CdSe/CdS g-QDs.[14,15] According to these earlier works, the biexciton PL QY progressively increases with the number of CdS MLs and could reach near-unity values in some individual QDs within a sample with an average shell thickness of 19 MLs. This previous finding seems to be at odds with the results of the present study, which does not show a significant dependence of Q_{BX} on shell thickness for either reference or alloyed QDs. This apparent discrepancy, however, can be easily explained if one accounts for the difference in samples used in these two studies. In the present work, we apply a fast shell-growth[21] that allows us to deposit an arbitrarily thick CdS shell with or without a well-defined layer of a mixed composition at the interface with the CdSe core. Given the key role played by interfacial alloying in these suppression of Auger decay, samples containing the layer of mixed composition start to show signatures of significant suppression of Auger recombination even at very small thicknesses of the CdS shell. Importantly, since this new synthesis requires drastically shorter reaction times, the shell growth is not accompanied by any appreciable, unintentional changes in the structure or thickness of the intermediate alloyed layer. Therefore, the increase in H does not lead to significant changes in biexciton lifetimes or emission efficiencies. This situation is in contrast to our previous studies in which we used the slow-growth SILAR method where the steps of interfacial alloying and the shell growth are not separated. Specifically, during SILAR the deposition of the CdS shell is accompanied by slow and largely uncontrolled build-up of an interfacial $CdSe_xS_{1-x}$ alloy layer due to uncontrolled interdiffusion of the S^{2-} and Se^{2-} ions[13] during prolonged growth times at elevated temperatures. As a result, significant interfacial alloying is only

dx.doi.org/10.1021/nl403289w | Nano Lett. 2014, 14, 396−402

achieved for large shell thicknesses, which leads to a delayed onset (*H*-wise) of appreciable suppression of Auger decay that, in turn, creates ambiguity regarding whether alloying or shell-thickness is ultimately responsible, ambiguity that the present study removes.

As should be expected, in addition to providing significant suppression of Auger decay for small shell thicknesses the new QDs with controlled interfacial alloying show a more uniform suppression of Auger decay across a QD ensemble than SILAR-grown samples. In Figure 3d, we compare relative biexciton emission efficiencies of similarly sized QDs with intentional alloying to those of traditional g-QDs. Although the average Q_{BX}/Q_X ratio of the alloyed QDs is lower than that of the g-QDs (0.1 versus 0.2), the controlled modification of the core/shell interface results in the reduced Q_{BX}/Q_X variability that drops down to 26% versus 57% for g-QDs. This suggests that further refinement of the interface, for example, by introducing finer compositional grading over the thickness of the alloy layer, may result in Auger suppression comparable to or better than that seen in g-QDs with much less variability.

In conclusion, we have performed single-dot PL studies of the effect of controlled interfacial alloying on Auger recombination in core/shell CdSe/CdS QDs. By using second-order intensity-correlation measurements we demonstrate that by incorporating a thin 1.5 nm layer of $CdSe_xS_{1-x}$ alloy ($x \approx 0.5$) between the core and shell we can achieve up to a 10-fold enhancement in the biexciton emission efficiency indicating a significant suppression of Auger decay. This result is corroborated by the observation of a considerable lengthening of biexciton lifetimes, which is in a remarkable quantitative agreement with expectation based on the observed changes in Q_{BX}. We further observe that the increase in CdS shell thickness (under conditions when it is not accompanied by appreciable interfacial alloying) has only a weak effect on Auger lifetimes that can be accounted for by a trivial change in the electron–hole overlap. These findings demonstrate the large potential of a new approach of interface engineering for reproducibly manipulating the rate of Auger decay and perhaps other Auger-type processes such as Auger ionization,[32] carrier multiplication,[33] and electron–hole energy transfer[34,35] without inducing significant changes in either spectral or dynamical properties of single-exciton emission.

■ ASSOCIATED CONTENT

Supporting Information

Additional information on structural characteristics of reference and alloyed QD samples as well as single-exciton and biexciton dynamics. This material is available free of charge via the Internet at http://pubs.acs.org.

■ AUTHOR INFORMATION

Corresponding Author

*E-mail: klimov@lanl.gov.

Present Addresses

[†]Instituto de Fisica "Gleb Wataghin", Universidade Estadual de Campinas, Unicamp, 13083-970, Campinas, Sao Paulo, Brazil.
[‡]Photo-Electronic Hybrid Research Center, Korea Institute of Science and Technology, Seoul 136-791, Korea.

Notes

The authors declare no competing financial interest.

■ ACKNOWLEDGMENTS

This work was supported by the Chemical Sciences, Biosciences and Geosciences Division of Office of Science, Office of Basic Energy Sciences, U.S. Department of Energy.

■ REFERENCES

(1) Klimov, V. I.; Mikhailovsky, A. A.; McBranch, D. W.; Leatherdale, C. A.; Bawendi, M. G. *Science* **2000**, *287*, 1011.
(2) Nirmal, M.; Dabbousi, B. O.; Bawendi, M. G.; Macklin, J. J.; Trautman, J. K.; Harris, T. D.; Brus, L. E. *Nature* **1996**, *383*, 802.
(3) Efros, A. L.; Rosen, M. *Phys. Rev. Lett.* **1997**, *78*, 1110.
(4) Colvin, V. L.; Schlamp, M. C.; Alivisatos, A. P. *Nature* **1994**, *370*, 354.
(5) Michler, P.; Imamoglu, A.; Mason, M. D.; Carson, P. J.; Strouse, G. F.; Buratto, S. K. *Nature* **2000**, *406*, 968.
(6) Lounis, B.; Bechtel, H. A.; Gerion, D.; Alivisatos, P.; Moerner, W. E. *Chem. Phys. Lett.* **2000**, *329*, 399.
(7) Nozik, A. J. *Physica E* **2002**, *14*, 115.
(8) Klimov, V. I.; Mikhailovsky, A. A.; Xu, S.; Malko, A.; Hollingsworth, J. A.; Leatherdale, C. A.; Eisler, H.-J.; Bawendi, M. G. *Science* **2000**, *290*, 314.
(9) Robel, I.; Gresback, R.; Kortshagen, U.; Schaller, R. D.; Klimov, V. I. *Phys. Rev. Lett.* **2009**, *102*, 177404.
(10) Klimov, V. I.; Ivanov, S. A.; Nanda, J.; Achermann, M.; Bezel, I.; McGuire, J. A.; Piryatinski, A. *Nature* **2007**, *447*, 441.
(11) Oron, D.; Kazes, M.; Banin, U. *Phys. Rev. B* **2007**, *75*, 035330.
(12) Zavelani-Rossi, M.; Lupo, M. G.; Tassone, F.; Manna, L.; Lanzani, G. *Nano Lett.* **2010**, *10*, 3142.
(13) Chen, Y.; Vela, J.; Htoon, H.; Casson, J. L.; Werder, D. J.; Bussian, D. A.; Klimov, V. I.; Hollingsworth, J. A. *J. Am. Chem. Soc.* **2008**, *130*, 5026.
(14) García-Santamaría, F.; Chen, Y.; Vela, J.; Schaller, R. D.; Hollingsworth, J. A.; Klimov, V. I. *Nano Lett.* **2009**, *9*, 3482.
(15) Park, Y.-S.; Malko, A. V.; Vela, J.; Chen, Y.; Ghosh, Y.; Garcia-Santamaria, F.; Hollingsworth, J. A.; Klimov, V. I.; Htoon, H. *Phys. Rev. Lett.* **2011**, *106*, 187401.
(16) Cragg, G. E.; Efros, A. L. *Nano Lett.* **2009**, *10*, 313.
(17) Climente, J. I.; Movilla, J. L.; Planelles, J. *Small* **2012**, *8*, 754.
(18) Wang, X.; Ren, X.; Kahen, K.; Hahn, M. A.; Rajeswaran, M.; Maccagnano-Zacher, S.; Silcox, J.; Cragg, G. E.; Efros, A. L.; Krauss, T. D. *Nature* **2009**, *459*, 686.
(19) Osovsky, R.; Cheskis, D.; Kloper, V.; Sashchiuk, A.; Kroner, M.; Lifshitz, E. *Phys. Rev. Lett.* **2009**, *102*, 197401.
(20) García-Santamaría, F.; Brovelli, S.; Viswanatha, R.; Hollingsworth, J. A.; Htoon, H.; Crooker, S. A.; Klimov, V. I. *Nano Lett.* **2011**, *11*, 687.
(21) Bae, W. K.; Padilha, L. A.; Park, Y.-S.; McDaniel, H.; Robel, I.; Pietryga, J. M.; Klimov, V. I. *ACS Nano* **2013**, *7*, 3411.
(22) Mahler, B.; Spinicelli, P.; Buil, S.; Quelin, X.; Hermier, J.-P.; Dubertret, B. *Nat. Mater.* **2008**, *7*, 659.
(23) Li, J. J.; Wang, Y. A.; Guo, W.; Keay, J. C.; Mishima, T. D.; Johnson, M. B.; Peng, X. *J. Am. Chem. Soc.* **2003**, *125*, 12567.
(24) Galland, C.; Ghosh, Y.; Steinbrück, A.; Hollingsworth, J. A.; Htoon, H.; Klimov, V. I. *Nat. Commun.* **2012**, *3*, 908.
(25) Mangum, B. D.; Ghosh, Y.; Hollingsworth, J. A.; Htoon, H. *Opt. Express* **2013**, *21*, 7419.
(26) Canneson, D.; Mallek-Zouari, I.; Buil, S.; Quélin, X.; Javaux, C.; Dubertret, B.; Hermier, J. P. *New J. Phys.* **2012**, *14*, 063035.
(27) Crooker, S. A.; Barrick, T.; Hollingsworth, J. A.; Klimov, V. I. *Appl. Phys. Lett.* **2003**, *82*, 2793.
(28) Brovelli, S.; Schaller, R. D.; Crooker, S. A.; García-Santamaría, F.; Chen, Y.; Viswanatha, R.; Hollingsworth, J. A.; Htoon, H.; Klimov, V. I. *Nat. Commun.* **2011**, *2*, 280.
(29) Nair, G.; Zhao, J.; Bawendi, M. G. *Nano Lett.* **2011**, *11*, 1136.
(30) Zhao, J.; Chen, O.; Strasfeld, D. B.; Bawendi, M. G. *Nano Lett.* **2012**, *12*, 4477.
(31) McGuire, J. A.; Joo, J.; Pietryga, J. M.; Schaller, R. D.; Klimov, V. I. *Acc. Chem. Res.* **2008**, *41*, 1810.

(32) Klimov, V. I.; McBranch, D. W. *Phys. Rev. B* **1997**, *55*, 13173.
(33) Schaller, R. D.; Klimov, V. I. *Phys. Rev. Lett.* **2004**, *92*, 186601.
(34) Efros, A. L.; Kharchenko, V. A.; Rosen, M. *Solid State Commun.* **1995**, *93*, 281.
(35) Klimov, V. I.; McBranch, D. W. *Phys. Rev. Lett.* **1998**, *80*, 4028.